RESEARCH ARTICLE

Highly efficient nickel (II) removal by sewage sludge biochar supported α-Fe$_2$O$_3$ and α-FeOOH: Sorption characteristics and mechanisms

Lie Yang[1,2], **Liuyang He**[1], **Jianming Xue**[2], **Li Wu**[1]*, **Yongfei Ma**[1], **Hong Li**[1], **Pai Peng**[1], **Ming Li**[1], **Zulin Zhang**[1,3]*

1 Hubei Key Laboratory of Mineral Resources Processing and Environment, School of Resources and Environmental Engineering, Wuhan University of Technology, Wuhan, PR China, **2** New Zealand Forest Research Institute Limited (Scion), Forest System, Christchurch, New Zealand, **3** The James Hutton Institute, Craigiebuckler, Aberdeen, United Kingdom

* wuli774@126.com (Li Wu); Zulin.Zhang@hutton.ac.uk (Zulin Zhang)

Abstract

A novel approach was employed to load α-Fe$_2$O$_3$ and α-FeOOH onto sewage sludge biochar (SBC) with the purpose of efficient nickel (Ni) removal. A high Ni(II) adsorption capacity of 35.50 mg·g^{-1} in 100 ppm Ni(II) solution with 10 mg modified sewage sludge biochar (MSBC) was achieved. The adsorption kinetic and isotherm were fitted well by the pseudo-second-order model and the Langmuir model, respectively. The optimal pH was found around a neutral pH of 7. The adsorption mechanisms of Ni(II) onto MSBC were described as the synergistic effects of electrostatic attraction, ion exchange, inner-sphere complexation and co-precipitation. The initial rapid adsorption phenomenon could be attributed to electrostatic attraction and ion exchange, and then inner-sphere complexation and co-precipitation acted as a crucial role in the following step. The remarkable performance of MSBC provides an effective waste utilization approach to simultaneous sewage sludge recycle and Ni removal from aqueous solution.

Introduction

Nickel (II) ion (Ni (II)), a toxic heavy metal ion, is discharged into natural waters mainly from various chemical industries, including textile dyeing, electroplating, and metal finishing [1]. Once the concentration of Ni(II) increases to a limit in the water bodies, there is a potential threat to food security and human health. An investigation was conducted in eastern Taiwan to evaluate the health risks of Ni in rice, and much higher Ni concentrations were observed in rice grain from Ni contaminated fields [2]. Furthermore, the incidence of oral cancer was found correlated positively with levels of Ni in farm soils based on a compulsory national health insurance program in Taiwan [3]. Soil contamination with Ni was frequently caused by

discharge of Ni wastewater without appropriate treatment. Therefore, effective and economical technologies for the Ni removal in wastewater are urgently needed.

So far, numerous attempts were made to eliminate Ni contamination, including chemical precipitation [4], phytoremediation [5], redox [6] and adsorption [7, 8]. Among them, adsorption is an effective technology for Ni removal and potentially for Ni recycle based on desorption [9]. In recent years, adsorbents derived from various wastes including agricultural and municipal wastes [10, 11], have attracted great attention due to the preference of waste disposal and recycle. Among diverse wastes, sewage sludge is a potential source for adsorbents due to its huge annual production from municipal wastewater treatment plants. However, raw sewage sludge is water swelling and generally contains various pollutants [12, 13]. Therefore, appropriate treatment is necessary to make this common solid waste to be a stable and safe adsorbent. There have been several studies focused on sewage sludge treatment especially for biochar production [14–16]. Pyrolysis of sewage sludge offers the advantage of releasing less flue gas that has to be managed as compared to incineration of sewage sludge and biochar can be obtained as potential adsorbents from the pyrolysis process [17]. Additionally, engineered (smart) biochar production from sewage sludge and willow has been attempted based on various carrying gases and mixture ratios of sludge and willow [18]. It is common that the biochar with appropriate modification presents higher surface areas and larger adsorption capacities than the raw wastes [19]. There has been several studies concerning Ni adsorption of biochar derived from bio-wastes except sewage sludge. For the sludge-derived biochar application, the research objective and modified methods of the relevant studies were mostly suitable for lead [14], cadmium [16], and some organic pollutants [20] rather than Ni.

In recent years, special attention was paid to α-Fe₂O₃ [21, 22] and α-FeOOH [23, 24] modification of adsorbents due to the outstanding improvement of the adsorption capacity. O-H was confirmed to be beneficial for copper adsorption [23] and it was found that 4–10 iron-bonded hydroxyl groups per nm² existed on the surface of α-Fe₂O₃ [25]. In addition, the interaction between α-FeOOH and Cu^{2+} was found possibly via the formation of Fe-O-Cu complexes [23], indicating that heavy metal ions could react with Fe-OH. The above characteristics of α-Fe₂O₃ and α-FeOOH are potential for enhancing the Ni adsorption from aqueous solution like Cu^{2+}. Until now, no systematic study concerning the adsorption performance of biochar with α-Fe₂O₃ and α-FeOOH in Ni (II) removal from aquatic environment has been published yet. To develop sewage sludge biochar for efficient Ni removal, we prepared sludge biochar (SBC) and then modified sludge biochar (MSBC) with α-Fe₂O₃ and α-FeOOH for Ni adsorption in aqueous solution. BET, XRD, SEM-EDS and FTIR were employed to characterize the prepared biochar. Dosages and pH were tested for the influences of adsorption parameters. In addition to the adsorbent regeneration, sorption kinetics and isotherms were assessed for the adsorption mechanisms in aqueous solution. This study could provide an efficient approach for simultaneously Ni removal and sludge application.

Material and methods

Materials

Iron(III) chloride hexahydrate (FeCl₃·6H₂O, ≥99%), iron(II) sulfate heptahydrate (FeSO₄·7H₂O, ≥99%), Ni nitrate(≥99%), sodium hydroxide (≥96%) and hydrochloric acid (36%) were purchased from Sinopharm Chemical Reagent Co., Ltd. (Shanghai, China). All reagents used in the experiments were of analytical grade and solutions were prepared with deionized water. The sewage sludge was provided by Tangxunhu Municipal Wastewater Plant in Wuhan, China. The obtained sludge was oven dried at 60 ˚C for 24 h and then went through slow pyrolysis at 500 ˚C with a heating rate of 10 ˚C·min⁻¹ for 2 h to produce the sludge

biochar (SBC). The obtained SBC was milled and then sieved (<0.074 mm) for further experiments.

Preparation of modified sludge biochar

The modified sludge biochar (MSBC) was fabricated based on SBC with the following procedure. $FeCl_3 \cdot 6H_2O$ (40 g) and $FeSO_4 \cdot 7H_2O$ (22.2 g) were dissolved in 1200 mL deionized water and then 30 g SBC was added into the solution. The mixture was stirred at room temperature (25 ~ 30 ˚C) for 30 min. Subsequently, 10 M NaOH solution was added into the mixture until the pH reached 10 and stirred for 2 h. After precipitation, the mixture was filtrated and the residual was washed with deionized water and ethanol several times and dried at 70 ˚C for 24 h. The obtained MSBC powder (0.074 mm) was kept for further experiments.

Characterizations

The surface area, pore width and pore volume of SBC and MSBC were measured with a Micromeritics ASAP 2020 analyzer (USA). The crystalline structure analysis was conducted with D8 X-ray diffraction spectra (Bruker, Germany). Fourier-transform infrared spectroscopy (FTIR) spectra were obtained with IRprestige-21 (Shimadzu, Japan) using the KBr pellet method and examined in the 4000–400 cm^{-1} region. The software named OMNIC was applied to analyze the FTIR spectra. The surface morphologies of the powder samples were analyzed by a JSM-7100F SEM (JEOL, Japan).

Batch experiments

To measure the adsorption capacities of SBC and MSBC adsorbents, 10–100 mg of these adsorbents were added to 50 ml of Ni(II) solution (100 ppm) at 25 ˚C for 24 h. Various pH values (2–7) were set to find the optimal pH for Ni(II) removal. The pH was adjusted to the desired values by using 0.01 M NaOH and HCl. Kinetic experiments were conducted by adding 50 mg MSBC adsorbent to 50 ml of Ni(II) solution (100 ppm) at 25 ˚C for various time intervals (2, 5, 10, 30 min and 1, 4, 8, 12, 18 h). The vials were sealed and shaken in a constant temperature shaker for 18 h to obtain the adsorption equilibrium. Correspondingly, an adsorption isotherm study was conducted by adding 50 mg of MSBC with 50 ml of Ni(II) solution (20–1000 ppm) at 25 ˚C. Finally, the desorption experiment was carried out using Na₂EDTA solution. The Ni loaded MSBC was soaked in 0.1 M Na₂EDTA solution and shaken for 2 h. And then, the Ni-desorbed MSBC was employed for further recycle experiments. The concentrations of Ni(II) solutions were measured by a 700P atomic absorption spectroscopy (Analytik Jena, Germany). The amount of adsorbed Ni(II) was calculated according to a previous study [14]. SPSS 19.0 and Microsoft Excel 2010 were used for data analysis in the kinetics and isotherm study, and Origin 8.0 was applied for graphing.

Results and discussion

Characterizations

The surface area, pore width and pore volume results of SBC and MSBC are presented in Table 1. The pore volume and pore width of SBC were larger than those of MSBC, while MSBC had a larger surface area (S_{BET}). As reported in previous studies, S_{BET} is critical for the adsorption of heavy metals including Ni [14, 26–28]. In this study, the widely distributed iron compounds on the surface of MSBC significantly increased S_{BET} of MSBC (34.99 m$^2 \cdot$g^{-1}). The higher S_{BET} of MSBC was of significant benefits to the adsorption capacity for Ni removal

Table 1. Pore distribution properties and Ni adsorption capacity of SBC and MSBC.

Biochar	pH	S_{BET} (m^2·g^{-1})	Pore volume ^{a} (cm^3·g^{-1})	Pore width (Å)	Adsorption capacity^b (mg/g)
SBC	8.12	24.21	0.0837	138.33	20.38
MSBC	8.73	34.99	0.0802	91.68	35.50

^{a} Pore Volume determined at P/Po = 0.99;

^{b} Adsorption average pore width (4V/A by BET).

(Table 1). The reduction of the pore volume and pore width during the fabrication of MSBC could be attributed to the occupation of iron compounds into the pores of the biochar.
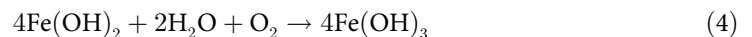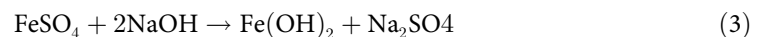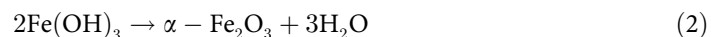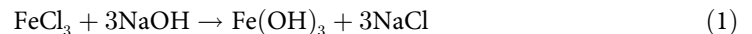
The XRD patterns of crystalline structures and composition of SBC and MSBC are shown in S1 Fig. Sharp reflection peaks at 20.86°, 26.30°, 36.55°, 42.14°, 50.15°, 60.00° and 68.08° in SBC and MSBC could be indexed as the planes of SiO$_2$ (PDF#65–0466), which were in line with the data in a previous study [29]. Therefore, SiO$_2$ could be reasonably considered as the dominating crystalline phase in both of SBC and MSBC. Furthermore, several peaks at 27.91°, 34.79°, 39.12°, 40.25°, 45.90°, 54.95° and 19.80°, 36.50°, 55.80°, 60.00° for MSBC revealed the formation of α-Fe$_2$O$_3$ (PDF#16–0653) and α-FeOOH (PDF#26–0792), respectively. The formation processes could be described by reactions (1)–(5). These reactions were confirmed by a previous study by Xiong and Zhou [30]. It has been demonstrated that Fe(OH)$_3$ can produce the mixture of FeOOH and α-Fe$_2$O$_3$ at the range of 40–80 °C, but only α-Fe$_2$O$_3$ at above 80°C [30]. The drying temperature was set at 70°C in this study, which could probably explain the observed crystalline phases.

$$FeCl_3 + 3NaOH \rightarrow Fe(OH)_3 + 3NaCl \tag{1}$$

$$2Fe(OH)_3 \rightarrow \alpha - Fe_2O_3 + 3H_2O \tag{2}$$

$$FeSO_4 + 2NaOH \rightarrow Fe(OH)_2 + Na_2SO4 \tag{3}$$

$$4Fe(OH)_2 + 2H_2O + O_2 \rightarrow 4Fe(OH)_3 \tag{4}$$

$$Fe(OH)_3 \rightarrow \alpha - FeOOH + H_2O \tag{5}$$
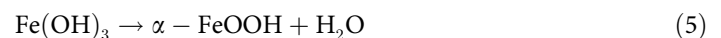
The external morphology of SBC and MSBC at both 5000 and 10000 magnifications are presented in S2 Fig. Obvious pore structures were observed on the surfaces of both SBC and MSBC. However, the conspicuous particles were only distributed on the surface of MSBC (S2 (c) and S2(d) Fig) but not SBC. These particles could be confirmed as iron oxides based on the above XRD analysis and SEM-EDS images in Fig 1. In addition, significant reduction of pore width on the surface of MSBC can be observed due to the occupation of iron compounds into the pores of adsorbents. This phenomenon was in agreement with the results of BET analysis (Table 1). The SEM-EDS images are presented in Fig 1, which revealed the characteristics of iron and Ni distribution on the surface of SBC and MSBC. It was observed that iron compounds distributed on the surface of SBC and MSBC and the iron percentage of MSBC was distinctly higher than that of SBC due to the fabrication process. It was worth noting that the Ni adsorption amount of MSBC was evidently higher compared with SBC (Fig 1). Furthermore, the Ni distribution locations appeared nearly consistent with the locations of the iron distribution. This provided evidence for the positive effects of α-Fe$_2$O$_3$ and α-FeOOH micro particles on Ni adsorption.
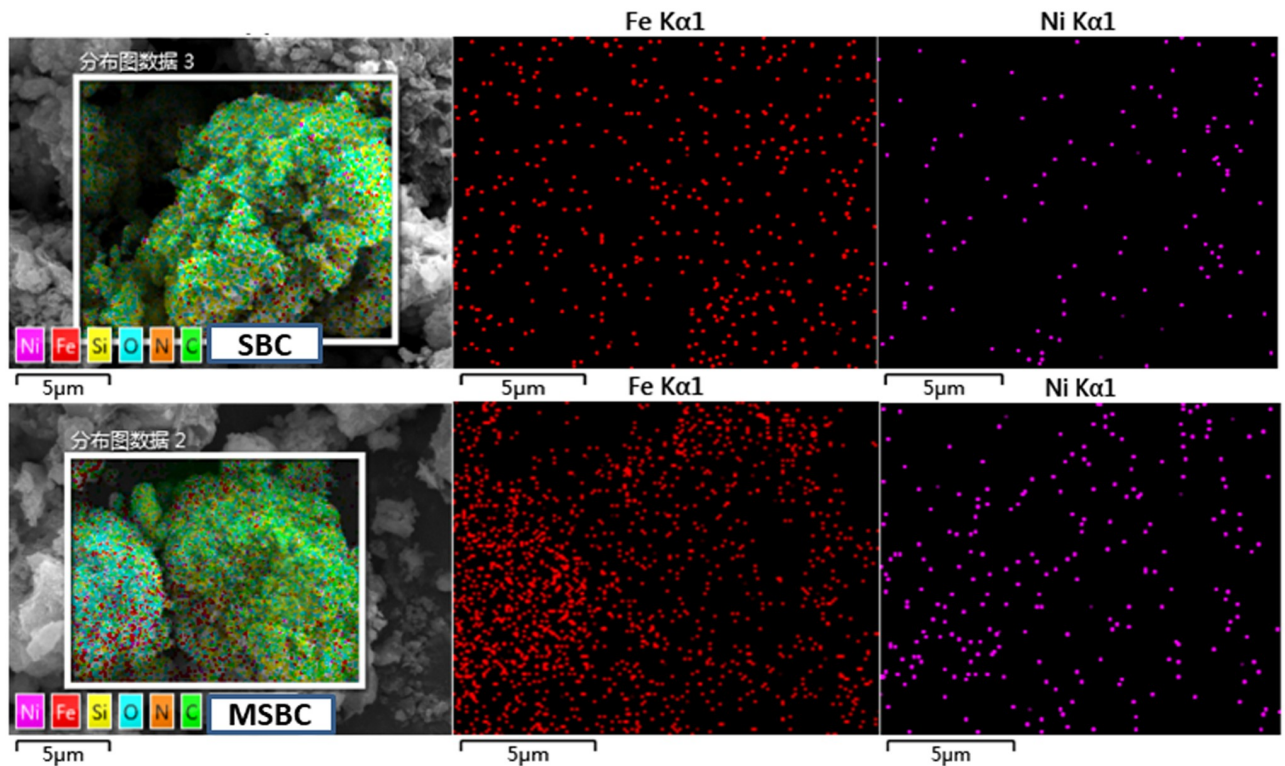
Fig 1. SEM-EDX analysis on the surface of SBC and MSBC after Ni adsorption.

https://doi.org/10.1371/journal.pone.0218114.g001

The FTIR spectra of SBC and MSBC before and after Ni adsorption are showed in S3 and S4 Figs. As for SBC, the spectrum before sorption shows the adsorption bonds at 3379 cm^{-1}, 1620 cm^{-1} and 1037 cm^{-1} for O-H, C = C and C-O, respectively [14, 31]. The band at 1080 cm^{-1} could be the P-O stretching vibrations of PO_4^{3-} [32, 33]. The bands at 797 cm^{-1} and 474 cm^{-1} were attributed to the deformation and bending modes of the Si-O bond [34, 35]. The slight peak at 551 cm^{-1} could be attributed to the Fe-O stretching vibration in α-Fe₂O₃ [34, 36], which indicated that there was original α-Fe₂O₃ in SBC. The spectra of MSBC was similar to that of SBC for strong bonds. An additional signal at 602 cm^{-1} could be assigned to the Fe-OH bending vibrations [23, 37], which was the solid evidence for the existence of α-FeOOH. These results further supported the findings obtained from XRD analysis.

Adsorption study

Adsorption capacity. Undoubtedly, adsorption capacity is a crucial parameter for adsorbents. Various studies have been conducted to develop novel adsorbents with efficient adsorption performance [38–40]. The comparison of SBC and MSBC adsorption capacities with various dosages for Ni removal is presented in Fig 2. It was evident that the adsorption capacity of MSBC was significantly higher than that of SBC at all dosage levels, which indicated that the fabrication procedure was effective for promotion of Ni adsorption. The maximum capacity of 35.50 mg·g^{-1} was achieved at the dosage of 0.01 g MSBC and decreased with the dose growth of adsorbent. Other biochar adsorbents were compared with SBC and MSBC for Ni removal (Table 2). It was obvious that the adsorption capacity of MSBC exceeded that of most biochar adsorbents as listed in Table 2. This remarkable performance could be due to multiple mechanisms between Ni ions and MSBC, which were discussed in Section 3.4.
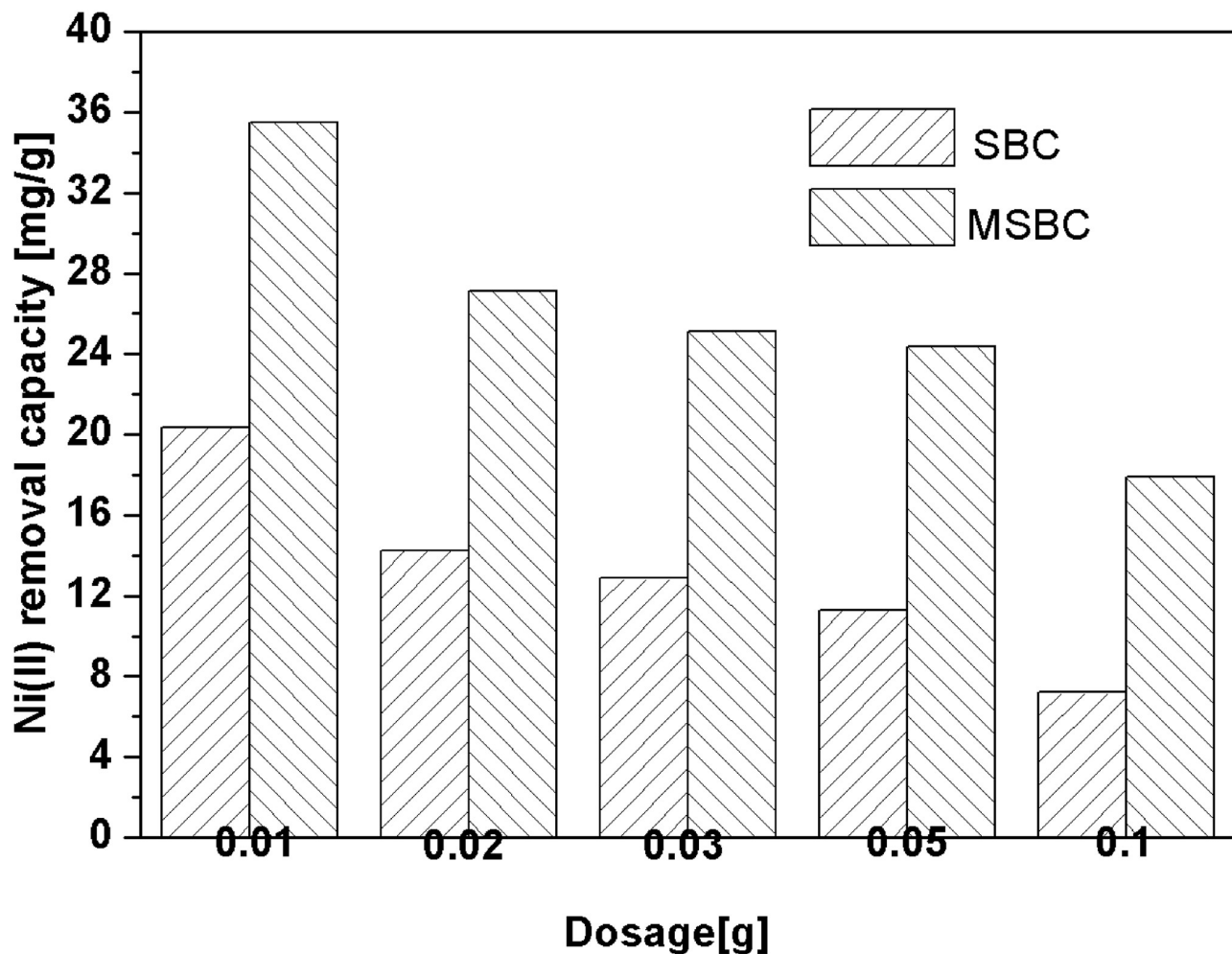
Fig 2. Comparison of SBC and MSBC adsorption capacities with various doses for Ni removal. Reaction conditions: Initial concentration of Ni(II) 100 ppm at pH 7, 50 ml of solution, 1~100 mg of biochar, 24 h, 25 ˚C.

Table 2. Comparison of the maximum adsorption capacity of Ni on SBC, MSBC and various pyrolysis biochars.

Biochar	Adsorption capacity of Ni (mg/g)	References
Palm seed-based biochar	28.00	[27]
Residues biochar	30.88	[41]
Chicken manure biochar	10.90	[42]
Wheat straw pellets biochar	22.89	[35]
Corncobs biochar	15.40	[8]
Corncobs biochar	29.06	[48]
Hizikia fusiformis biochar	10.39	[49]
Chrysanthemum indicum biochar	29.44	[50]
Sugarcane bagasse biochar (milled)	38.15	[51]
Sugarcane bagasse biochar (unmilled)	6.46	[51]
SBC	20.38	This study
MSBC	35.50	This study

Effect of pH. The increase from pH 2 to pH 7 caused the increase in the adsorption capacity of Ni(II) by both SBC and MSBC (Fig 3). The variations could be attributed to the differences of the surface groups of SBC and MSBC under different solution pH [41]. At a low pH (pH = 2), nearly no Ni(II) adsorption was observed due to the protonation of surface groups by H$^+$ ions derived from the solution [41]. It was believed that the deprotonation of the functional groups would occur resulting in less competition of the metal ions with protons for the same binding sites, thus leading to increases in the capture of metal ions on the surface of the biochar [42]. Therefore, Ni(II) ions could be bonded to the surface of the biochar with the increase of pH (pH = 2~5). In the pH range of 2~5, the Ni existed in the form of Ni(OH)$^+$, resulting lower electrostatic repulsion between the ion and the surface of the biochar [41]. A previous zeta potential analysis indicated that the zeta potential values of sewage sludge biochar were below -30 mV at pH 4~8 [14]. Thus strong electrostatic attraction would occur between electronegative biochar surface and cationic Ni^{2+} and Ni(OH)$^+$. According to Fig 3, slight increases were observed at pH>6, probably due to the precipitation of Ni(II) ions on the surface of biochar in the form of hydroxides. This phenomenon was also observed in a previous Ni(II) adsorption study [35]. The pH$_{pzc}$ values of biochar were found within the range of 7.3–7.8 [35]. Overall, neutral initial pH 7 is beneficial for wastewater treatment. Therefore, pH 7 is the optimal value for Ni(II) adsorption in this study.

Sorption kinetics. The adsorption kinetics of MSBC on Ni(II) removal are shown in Fig 4. The parameter of q$_t$ represents the adsorbed amount of Ni(II) at a certain time. The adsorption amount of Ni(II) gradually increased and reached an equilibrium level within 18 hours. It was noticed that the adsorption of Ni(II) achieved nearly 50% of the maximum adsorption capacity at 100 ppm concentration of Ni(II) within 2 min. Several previous studies reported the similar adsorption process when biochar was utilized to adsorb heavy metal ions [35]. The rapid adsorption phenomenon could be attributed to electrostatic attraction and ion exchange, which took a few minutes to reach equilibrium based on available literatures [43]. The pseudo-first-order and pseudo-second-order models were employed to investigate the adsorption kinetic as shown in the equation below:

$$\ln(q_e - q_t) = \ln q_e - k_1 t \tag{6}$$

$$t/q_t = 1/(k_2 q_e^2) - t/q_e \tag{7}$$

Where k$_1$ represents the pseudo-first-order rate constant (min^{-1}), k$_2$ is the pseudo-second-order rate constant (g/mg·min^{-1}) of adsorption, q$_e$ and q$_t$ are the amounts of Ni(II) adsorbed on MSBC (mg·g^{-1}) at equilibrium and at time t, respectively.

The above parameters were obtained through curve fitting and presented in Table 3. The plotting of the graph ln (q$_e$-q$_t$) versus time (t) for the pseudo-first-order kinetic model did not yield good convergence (R^2 0.9435). In this regard, the correlation coefficient (R^2 = 0.9995) of the pseudo-second-order model was remarkably higher than that of pseudo-first-order model. Furthermore, the equilibrium adsorption amount (q$_e$) of the pseudo-second-order model (24.45 mg·g^{-1}) was close to the experiment data (24.55 mg·g^{-1}). Therefore, the kinetic analysis revealed the chemical adsorption of Ni onto MSBC was the dominating mechanism.

Sorption isotherm. As shown in Fig 5, the increased initial Ni(II) concentration (Ce) resulted in increased equilibrium adsorption capacity (Q$_e$). Once the C$_e$ reached above 800 ppm, no further increase was observed for Q$_e$. The Langmuir and Freundlich models, frequently used in various adsorption studies [11, 39], were employed to simulate the isotherm of Ni(II) on MSBC (Table 3). Obviously, the experimental data was well fitted by the Langmuir model with an R^2 value of 0.9930, while that of the Freundlich model was 0.9821. Actually, the
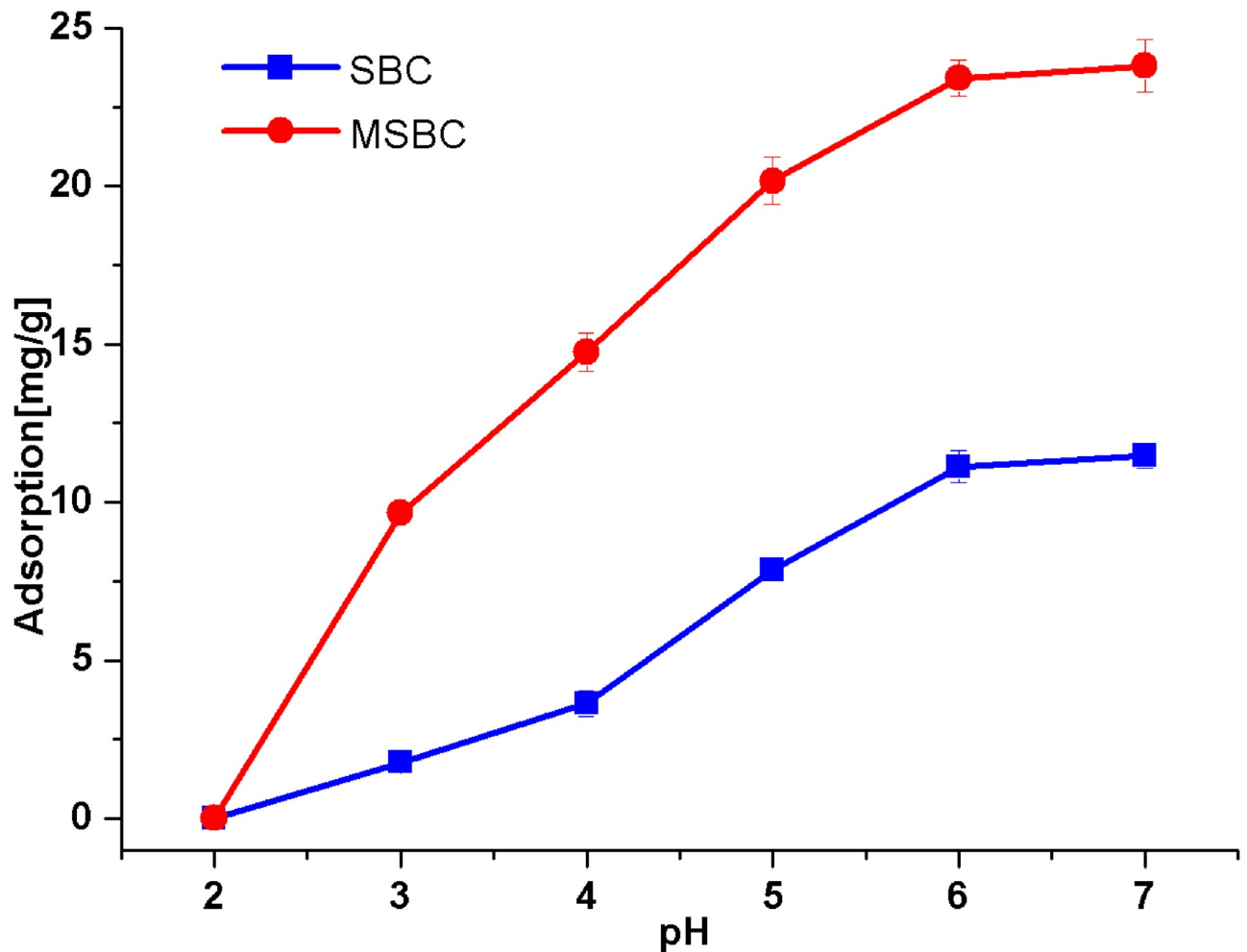
Fig 3. The influence of initial pH on adsorption of Ni(II) solution. Reaction conditions: Initial concentration of Ni(II) 100 ppm at pH 2~7, 25 ml of solution, 50 mg of SBC and MSBC, 24 h, 25 ˚C.

https://doi.org/10.1371/journal.pone.0218114.g003

adsorption path of the Langmuir model was believed to be monolayer sorption on a homogeneous sorption surface [40]. Nevertheless, the Freundlich model can be regard as non-ideal sorption on a heterogeneous surface as well as multilayer sorption [40]. As mentioned above, the R^2 value of the Langmuir model was slightly higher than that of the Freundlich model. The calculated values of Ni(II) adsorption capacity were 35.97 mg·g^{-1} (Q_m) and 10.50 mg·g^{-1} (K_L), respectively for the Langmuir and Freundlich models. Comparing to the adsorption capacity of MSBC (Table 2), Q_m was much closer to 35.50 mg·g^{-1} than K_L. This suggested that monolayer sorption on a homogeneous sorption surface could be dominant in our experiments.

Recycle and desorption performance

The regeneration capability of the biochar is vital for further application from an economic point of view. Desorption attempts could be applied to recycle the metal ions and regenerate the saturated adsorbents. Thermal activation and acid solution were reported as regeneration methods based on previous literatures [40, 44]. High energy requirement and adsorbent loss were noticed in thermal activation attempts of the saturated adsorbent [44]. Acid desorption may cause negative impact of the adsorption abilities and structure of the regenerated biochar
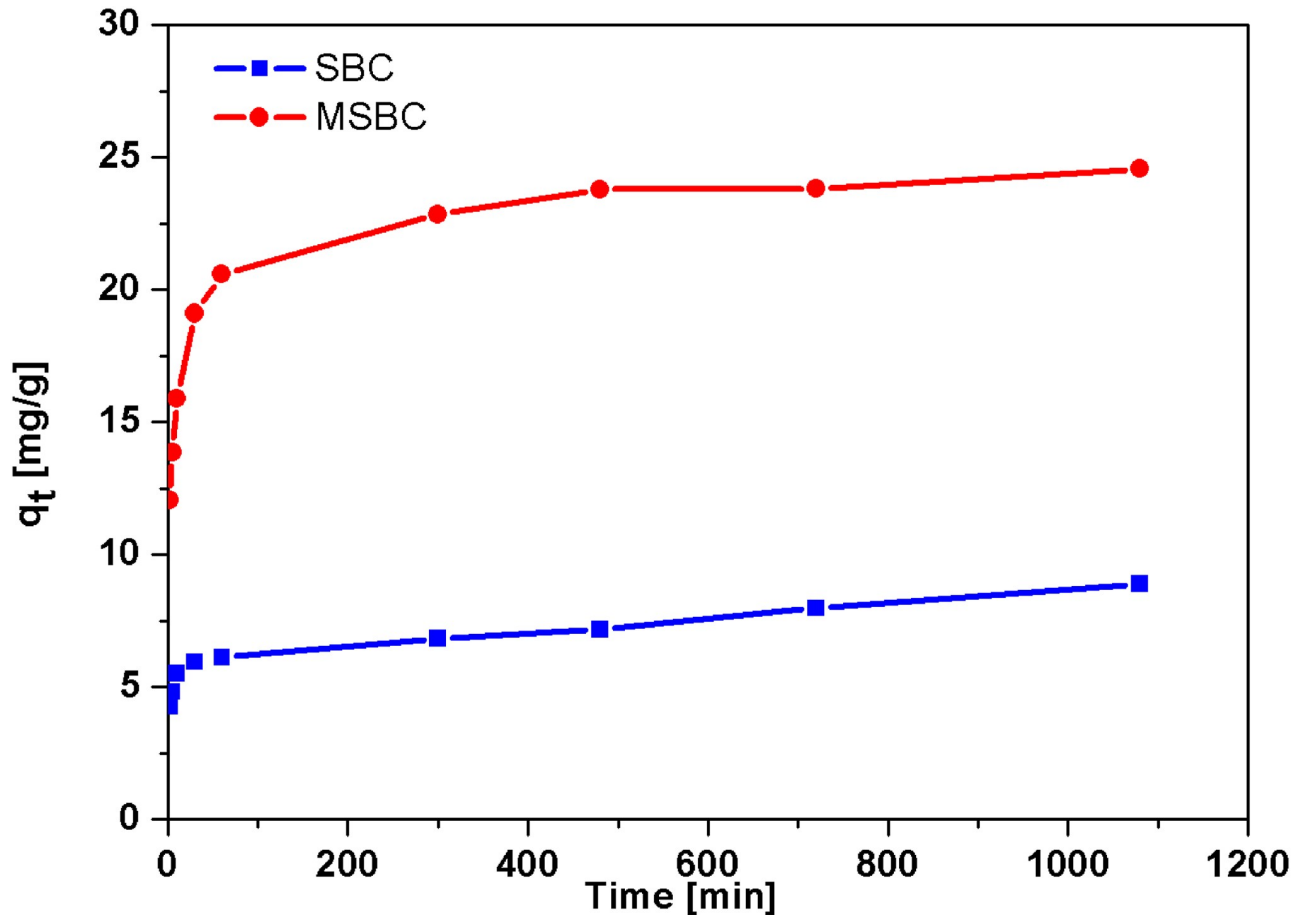
Fig 4. The kinetic of Ni(II) adsorption onto SBC and MSBC. Reaction conditions: Initial concentration of Ni(II) 100 ppm at pH 7, 50 ml of solution, 50 mg of MSBC, 18 h, 25 ˚C.

[40]. So far Na₂EDTA was found effective in the desorption of Pb(II) from the saturated biochar with less negative effects[14]. In this study, 0.1 M Na₂EDTA was employed as a desorption agent. The adsorption and desorption efficiencies of MSBC for five cycles are shown in Fig 6. It was observed that the removal efficiency remained 60% and the desorption efficiency still achieved around 90% in the fifth cycle. The remarkable performance of MSBC demonstrated excellent regeneration potential, which presented the prospect of its expanding lifespan. The contents of typical heavy metals in SBC and MSBC were also investigated (S1 Table). Compared with the threshold values for sewage sludge used in forestland, all the heavy metals

Table 3. Parameters of kinetic and isotherm models for Ni adsorption onto MSBC.

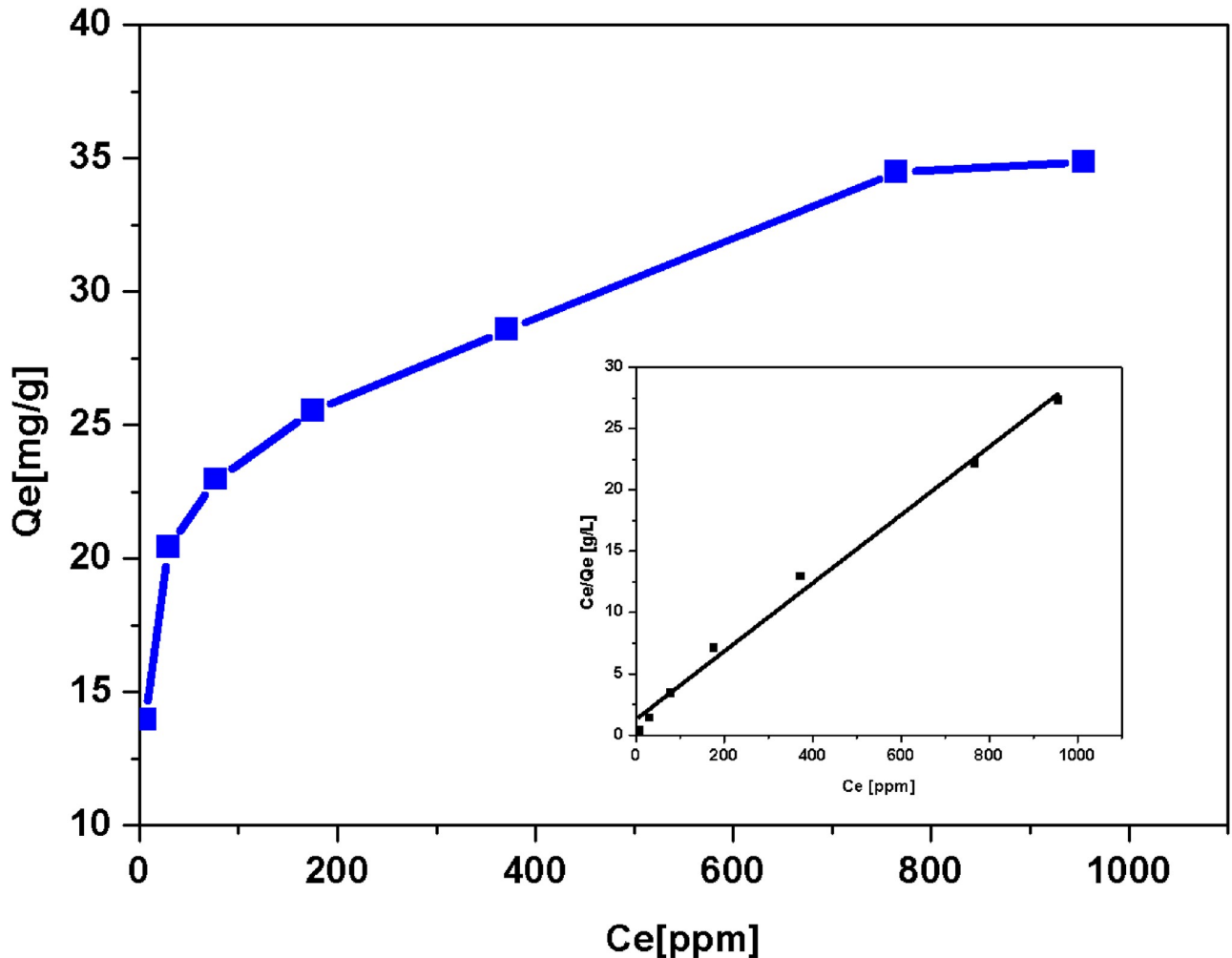|	Parameter 1	Parameter 2	R^2
Adsorption kinetics			
Pseudo-first-order	$k_1 = 4.0\times10^{-3}\,min^{-1}$	$q_e = 8.07\,mg\cdot g^{-1}$	0.9435
Pseudo-second-order	$k_2 = 6.31\times10^{-4}\,g\cdot mg\cdot min^{-1}$	$q_e = 24.45\,mg\cdot g^{-1}$	0.9995
Adsorption isotherm			
Langmuir	$K_L = 3.56\times10^{-2}\,L\cdot mg^{-1}$	$Q_m = 35.97\,mg\cdot g^{-1}$	0.9930
Freundlich	$n = 5.7438$	$K_F = 10.50\,mg\cdot g^{-1}$	0.9821

Fig 5. The isotherm of Ni(II) adsorption onto MSBC. Reaction conditions: Initial concentration of Ni(II) 20–1000 ppm at pH 7, 50 ml of solution, 50 mg of MSBC, 24 h, 25 ˚C.

contents in the SBC and MSBC were lower than those in the Chinese standard [45]. In addition, the exchangeable and acid-soluble fraction and the reducible fraction of heavy metals could be decreased via pyrolysis [46]. Overall, the MSBC adsorbent produced in this study is safe for the natural environment.

Adsorption mechanism

The mechanism of Ni(II) adsorption on adsorbents was believed to be the synergistic effect of physical and chemical adsorptions [7]. The high surface areas and pore structure of MSBC were observed based on BET and SEM analysis. Besides, batch experiments at various pH values indicated that the electrostatic attraction occurred in the adsorption process. However, the dominant role was proved to be chemical adsorption rather than physical adsorption based on our kinetic study. Similar results were reported in other Ni(II) adsorption studies [47]. Furthermore, the adsorption isotherm analysis revealed monolayer sorption on a homogeneous sorption surface could be dominant in the experiments. The initial rapid adsorption phenomenon could be attribute to electrostatic attraction and ion exchange, and chemical adsorption
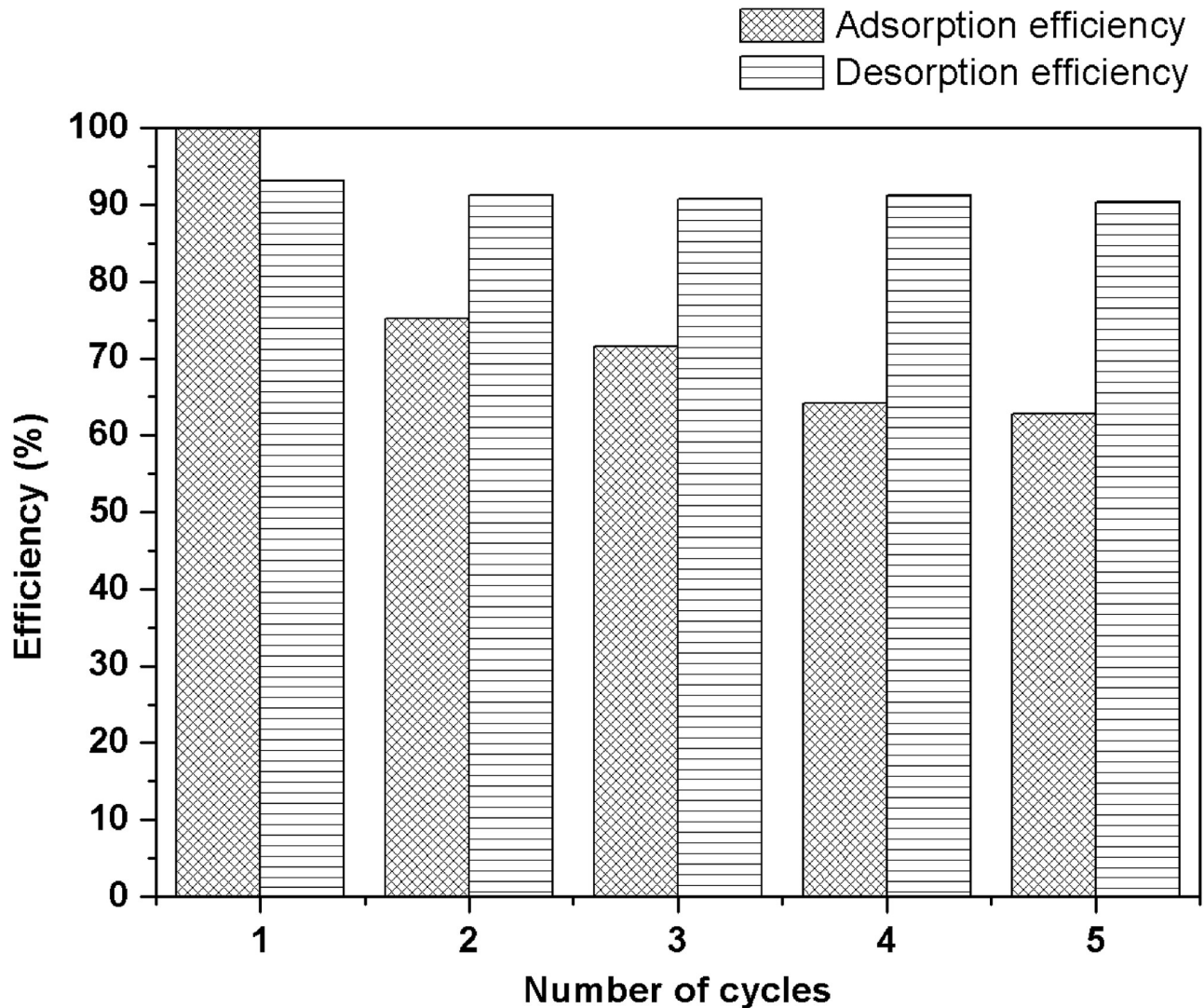
Fig 6. Ni(II) adsorption or desorption efficiencies of MSBC at five regeneration cycles.

acted as a crucial role in the following step [14]. The chemical reactions of heavy metal adsorption were generally defined as inner-sphere complexation and co-precipitation [47]. The solution after Ni(II) adsorption was detected by ICP-AES and K^+, Mg^{2+} and Ca^{2+} were found after the adsorption treatment, convincingly demonstrating the ion exchange between Ni(II) and aforementioned metal ions. Comparison analysis was achieved between the FTIR spectra of MSBC before and after Ni(II) adsorption (S4 Fig). Significant shifts were found from 3420 cm^{-1} to 3397 cm^{-1}, 1635 cm^{-1} to 1631 cm^{-1}, 1094 cm^{-1} to 1077 cm^{-1}, 1033 cm^{-1} to 1030 cm^{-1}, 796 cm^{-1} to 797 cm^{-1}, 780 cm^{-1} to 779 cm^{-1}, 693 cm^{-1} to 694 cm^{-1}, 548 cm^{-1} to 550 cm^{-1}, and 472 cm^{-1} to 475 cm^{-1}. The band change from 548 cm^{-1} to 550 cm^{-1} could be attributed to the O-H from α-Fe₂O₃, due to about 4–10 iron-bonded hydroxyl groups per nm^2 on the surface of α-Fe₂O₃ [25]. According to the wavelength variation of O-H, Ni(II) was probably bonded with free hydroxyl (O-H) functional groups by way of inner-sphere complexation like other heavy metal ions [14]. Meanwhile, co-precipitation reaction between Ni(II) and PO_4^{3-} might occur, which was suggested by the peak variation from 1094 cm^{-1} to 1077 cm^{-1} (P-O). In addition, the

peak at 602 cm^{-1} disappeared after adsorption, which suggested the involvement of Fe-OH. The interaction between α-FeOOH and Cu^{2+} was found possibly via the formation of Fe-O-Cu complexes [23]. The formation of Fe-O-Ni complexes occurred probably during the adsorption process in this study. In short, inner-sphere complexation and co-precipitation could be confirmed based on the above FTIR analysis. Furthermore, the comparison of XRD patterns between MSBC before and after Ni(II) adsorption was conducted to understand the Ni formations via the crystalline structure analysis. The XRD patterns of Ni$_3$(PO$_4$)$_2$ (PDF#38–1473) and Ni(OH)$_2$ (PDF#38–0715) co-precipitations were identified by XRD analysis with the typical 2 theta of 24.12˚, 30.03˚, 38.20˚, 53.17˚, 63.89˚ and 22.61˚, 45.83˚, 59.93˚, 61.32˚, respectively (S5 Fig). The formation of Ni$_3$(PO$_4$)$_2$ and Ni(OH)$_2$ may be due to reactions (8) and (9). The outcome of XRD analysis was consistent with that of the FTIR spectra. The high content of inorganic phosphorus (S2 Table) in MSBC also supported the formation of Ni$_3$(PO$_4$)$_2$.

$$Ni^{2+} + 2OH^- \rightarrow Ni(OH)_2 \downarrow \tag{8}$$

$$3Ni^{2+} + 2(PO_4)^{3+} \rightarrow Ni_3(PO_4)_2 \downarrow \tag{9}$$
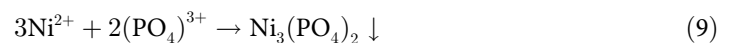
In conclusion, Ni adsorption was mainly attributed to electrostatic attraction, ion exchange, inner-sphere complexation and co-precipitation. Fast adsorption in the first several minutes was due to electrostatic attraction and ion exchange. And then the crucial mechanisms were inner-sphere complexation and co-precipitation.

Conclusions

Modified sewage sludge biochar (MSBC) was technically produced by distributing both α-Fe$_2$O$_3$ and α-FeOOH particles onto the surface of SBC. The maximum Ni adsorption capacity of MSBC reached 35.50 mg·g^{-1}. The adsorption process could be fitted by the pseudo-second-order model and adsorption isotherm was well described by the Langmuir model. The initial rapid adsorption phenomenon could be attributed to electrostatic attraction and ion exchange, and then inner-sphere complexation and co-precipitation acted as a crucial role in the following step. Although the mechanism of Ni(II) adsorption was believed to be the synergistic effect of physical and chemical adsorptions, the dominant role was proved to be chemical adsorption. The results in this study indicate that MSBC could act as an excellent adsorbent for Ni removal.

Supporting information

S1 Table. Total concentrations of heavy metals in samples and their threshold values for the disposal standards of China.
(DOC)

S2 Table. The inorganic phosphorus contents of SBC and MSBC.
(DOC)

S1 Fig. XRD patterns of SBC, MSBC before nickel adsorption.
(TIF)

S2 Fig. SEM images of (a) SSBC (X2000), (b) SSBC (X5000), (c) MSSBC (X2000) and (d) MSSBC (X5000).
(TIF)

S3 Fig. FTIR spectra of SBC and MSBC before nickel adsorption.
(TIF)

S4 Fig. FTIR spectra of MSBC before and after nickel adsorption.
(TIF)

S5 Fig. XRD spectra of MSBC after nickel adsorption.
(TIF)

S1 Data. Raw Data.
(ZIP)

Author Contributions

Data curation: Yongfei Ma, Hong Li, Ming Li, Zulin Zhang.

Formal analysis: Pai Peng.

Investigation: Liuyang He.

Supervision: Li Wu.

Writing – original draft: Lie Yang.

Writing – review & editing: Jianming Xue.

References

1. Vidhya L, Dhandapani M, Shanthi K. Sequestering Divalent Nickel Ions from Aqueous Solution Using Activated Carbon of Citrus limetta Peel: Isothermic and Kinetic Studies. Pol J Environ Stud. 2017; 26 (4):1737–1745. https://doi.org/10.15244/pjoes/69092

2. Hseu ZY, Lai YJ. Nickel accumulation in paddy rice on serpentine soils containing high geogenic nickel contents in Taiwan. Environ Geochem Hlth. 2017; 39(6):1325–1334. https://doi.org/10.1007/s10653-017-9925-6 PMID: 28229256

3. Lee CP, Lee YH, Lian IB, Su CC. Increased Prevalence of Esophageal Cancer in Areas with High Levels of Nickel in Farm Soils. J Cancer. 2016; 7(12):1724–1730. https://doi.org/10.7150/jca.15441 PMID: 27698910

4. Thomas M, Bialecka B, Zdebik D. Removal of copper, nickel and tin from model and real industrial wastewater using sodium trithiocarbonate. The negative impact of complexing compounds. Arch Environ Prot. 2018; 44(1):33–47. https://doi.org/10.24425/118179

5. Sima J, Svoboda L, Pomijova Z. Removal of Selected Metals from Wastewater Using a Constructed Wetland. Chem Biodivers. 2016; 13(5):582–590. https://doi.org/10.1002/cbdv.201500189 PMID: 27119624

6. Li CW, Yu JH, Liang YM, Chou YH, Park HJ, Choo KH, et al. Ni removal from aqueous solutions by chemical reduction: Impact of pH and pe in the presence of citrate. J Hazard Mater. 2016; 320:521–528. https://doi.org/10.1016/j.jhazmat.2016.08.030 PMID: 27597152

7. Alam MS, Gorman-Lewis D, Chen N, Flynn SL, Ok YS, Konhauser KO, et al. Thermodynamic Analysis of Nickel(II) and Zinc(II) Adsorption to Biochar. Environ Sci Technol. 2018; 52(11):6246–6255. https://doi.org/10.1021/acs.est.7b06261 PMID: 29746774

8. Hu XL, Xue YW, Liu LN, Zeng YF, Long L. Preparation and characterization of Na2S-modified biochar for nickel removal. Environ Sci Pollut R. 2018; 25(10):9887–9895. https://doi.org/10.1007/s11356-018-1298-6 PMID: 29372530

9. Ding ZH, Hu X, Wan YS, Wang SS, Gao B. Removal of lead, copper, cadmium, zinc, and nickel from aqueous solutions by alkali-modified biochar: Batch and column tests. J Ind Eng Chem. 2016; 33:239–245. https://doi.org/10.1016/j.jiec.2015.10.007

10. Lee XJ, Lee LY, Hiew BYZ, Gan SY, Thangalazhy-Gopakumar S, Ng HK. Multistage optimizations of slow pyrolysis synthesis of biochar from palm oil sludge for adsorption of lead. Bioresource Technol. 2017; 245:944–953. https://doi.org/10.1016/j.biortech.2017.08.175 PMID: 28946195

11. Jin H, Capareda S, Chang Z, Gao J, Xu Y, Zhang J. Biochar pyrolytically produced from municipal solid wastes for aqueous As(V) removal: Adsorption property and its improvement with KOH activation. Bioresource Technol. 2014; 169(Supplement C):622–629. https://doi.org/10.1016/j.biortech.2014.06.103.

12. Marchenko O, Demchenko V, Pshinko G. Bioleaching of heavy metals from sewage sludge with recirculation of the liquid phase: A mass balance model. Chem Eng J. 2018; 350:429–435. https://doi.org/10.1016/j.cej.2018.05.174

13. Zhou WB, Lu Y, Jiang S, Xiao YF, Zheng GY, Zhou LX. Impact of sludge conditioning treatment on the bioavailability of pyrene in sewage sludge. Ecotox Environ Safe. 2018; 163:196–204. https://doi.org/10.1016/j.ecoenv.2018.07.088 PMID: 30055384

14. Ifthikar J, Wang J, Wang QL, Wang T, Wang HB, Khan A, et al. Highly Efficient Lead Distribution by Magnetic Sewage Sludge Biochar: Sorption Mechanisms and Bench Applications. Bioresource Technol. 2017; 238:399–406. https://doi.org/10.1016/j.biortech.2017.03.133 PMID: 28458173

15. Wang J, Liao ZW, Ifthikar J, Shi LR, Chen ZQ, Chen ZL. One-step preparation and application of magnetic sludge-derived biochar on acid orange 7 removal via both adsorption and persulfate based oxidation. RSC Adv. 2017; 7(30):18696–18706. https://doi.org/10.1039/c7ra01425b

16. Zuo WQ, Chen C, Cui HJ, Fu ML. Enhanced removal of Cd(II) from aqueous solution using CaCO3 nanoparticle modified sewage sludge biochar. RSC Adv. 2017; 7(26):16238–16243. https://doi.org/10.1039/c7ra00324b

17. Paz-Ferreiro J, Nieto A, Mendez A, Askeland MPJ, Gasco G. Biochar from Biosolids Pyrolysis: A Review. Int J Env Res Pub He. 2018; 15(5): 956. https://doi.org/10.3390/ijerph15050956 PMID: 29748488

18. Konczak M, Oleszczuk P, Rozylo K. Application of different carrying gases and ratio between sewage sludge and willow for engineered (smart) biochar production. J CO₂ Util. 2019; 29:20–28. https://doi.org/10.1016/j.jcou.2018.10.019

19. Bakshi S, Banik C, Rathke SJ, Laird DA. Arsenic sorption on zero-valent iron-biochar complexes. Water Res. 2018; 137:153–163. https://doi.org/10.1016/j.watres.2018.03.021 PMID: 29554531

20. Wang B, Jiang YS, Li FY, Yang DY. Preparation of biochar by simultaneous carbonization, magnetization and activation for norfloxacin removal in water. Bioresource Technol. 2017; 233:159–165. https://doi.org/10.1016/j.biortech.2017.02.103 PMID: 28279909

21. Xu HJ, Zhang XP, Zhang YD. Modification of biochar by Fe2O3 for the removal of pyridine and quinoline. Environ Technol. 2018; 39(11):1470–1480. https://doi.org/10.1080/09593330.2017.1332103 PMID: 28555520

22. Zhu ZQ, Huang CP, Zhu YN, Wei WH, Qin H. A hierarchical porous adsorbent of nano-alpha-Fe2O3/Fe3O4 on bamboo biochar (HPA-Fe/C-B) for the removal of phosphate from water. J Water Process Eng. 2018; 25:96–104. https://doi.org/10.1016/j.jwpe.2018.05.010

23. Yang F, Zhang SS, Li HP, Li SS, Cheng K, Li JS, et al. Corn straw-derived biochar impregnated with alpha-FeOOH nanorods for highly effective copper removal. Chem Eng J. 2018; 348:191–201. https://doi.org/10.1016/j.cej.2018.04.161

24. Fu DD, He ZQ, Su SS, Xu B, Liu YL, Zhao YP. Fabrication of alpha-FeOOH decorated graphene oxide-carbon nanotubes aerogel and its application in adsorption of arsenic species. J Colloid Interf Sci. 2017; 505:105–114. https://doi.org/10.1016/j.jcis.2017.05.091 PMID: 28577460

25. Dewage NB, Liyanage AS, Pittman CU, Mohan D, Mlsna T. Fast nitrate and fluoride adsorption and magnetic separation from water on alpha-Fe2O3 and Fe3O4 dispersed on Douglas fir biochar. Bioresource Technol. 2018; 263:258–265. https://doi.org/10.1016/j.biortech.2018.05.001 PMID: 29753258

26. Wang SY, Tang YK, Li K, Mo YY, Li HF, Gu ZQ. Combined performance of biochar sorption and magnetic separation processes for treatment of chromium-contained electroplating wastewater. Bioresource Technol. 2014; 174:67–73. https://doi.org/10.1016/j.biortech.2014.10.007 PMID: 25463783

27. Gazi M, Oladipo AA, Azalok KA. Highly efficient and magnetically separable palm seed-based biochar for the removal of nickel. Separ Sci Technol. 2018; 53(7):1124–1131. https://doi.org/10.1080/01496395.2017.1340955

28. Zhang M, Gao B, Cao XD, Yang LY. Synthesis of a multifunctional graphene-carbon nanotube aerogel and its strong adsorption of lead from aqueous solution. RSC Adv. 2013; 3(43):21099–21105. https://doi.org/10.1039/c3ra44340j

29. Han ZT, Sani B, Mrozik W, Obst M, Beckingham B, Karapanagioti HK, et al. Magnetite impregnation effects on the sorbent properties of activated carbons and biochars. Water Res. 2015; 70:394–403. https://doi.org/10.1016/j.watres.2014.12.016 PMID: 25555224

30. Xiong H-x, Zhou L-x. Synthesis of iron oxyhydroxides of different crystal forms and their roles in adsorption and removal of Cr(VI)from aqueous solutions. Acta Petrol ET Miner. 2008; 27(6):559–566.

31. Yang JP, Zhao YC, Ma SM, Zhu BB, Zhang JY, Zheng CG. Mercury Removal by Magnetic Biochar Derived from Simultaneous Activation and Magnetization of Sawdust. Environ Sci Technol. 2016; 50 (21):12040–7. https://doi.org/10.1021/acs.est.6b03743 PMID: 27723318

32. Lee ME, Park JH, Chung JW. Adsorption of Pb(II) and Cu(II) by Ginkgo-Leaf-Derived Biochar Produced under Various Carbonization Temperatures and Times. Int J Env Res Pub He. 2017; 14(12):1528. https://doi.org/10.3390/ijerph14121528 PMID: 29215580

33. Xu Y, Huang MH, Luo XB. Enhanced phosphate adsorption performance by innovative anion imprinted polymers with dual interaction. Appl Surf Sci. 2019; 467:135–142. https://doi.org/10.1016/j.apsusc.2018.10.095

34. Ruan ZH, Wu JH, Huang JF, Lin ZT, Li YF, Liu YL, et al. Facile preparation of rosin-based biochar coated bentonite for supporting alpha-Fe2O3 nanoparticles and its application for Cr(VI) adsorption. J Mater Chem A. 2015; 3(8):4595–4603. https://doi.org/10.1039/c4ta06491g

35. Shen ZT, Zhang YH, McMillan O, Jin F, Al-Tabbaa A. Characteristics and mechanisms of nickel adsorption on biochars produced from wheat straw pellets and rice husk. Environ Sci Pollut R. 2017; 24 (14):12809–12819. https://doi.org/10.1007/s11356-017-8847-2 PMID: 28364204

36. Maziarz P, Matusik J, Leiviska T, Strazek T, Kapusta C, Woch WM, et al. Toward highly effective and easily separable halloysite-containing adsorbents: The effect of iron oxide particles impregnation and new insight into As(V) removal mechanisms. Sep Purif Technol. 2019; 210:390–401. https://doi.org/10.1016/j.seppur.2018.08.012

37. Andjelkovic I, Tran DNH, Kabiri S, Azari S, Markovic M, Losic D. Graphene Aerogels Decorated with alpha-FeOOH Nanoparticles for Efficient Adsorption of Arsenic from Contaminated Waters. ACS Appl Mater Inter. 2015; 7(18):9758–9766. https://doi.org/10.1021/acsami.5b01624 PMID: 25871444

38. Zhou YY, Liu XC, Xiang YJ, Wang P, Zhang JC, Zhang FF, et al. Modification of biochar derived from sawdust and its application in removal of tetracycline and copper from aqueous solution: Adsorption mechanism and modelling. Bioresource Technol. 2017; 245:266–273. https://doi.org/10.1016/j.biortech.2017.08.178 PMID: 28892700

39. Lu HP, Li ZA, Gascó, Méndez A, Shen Y, Paz-Ferreiro J. Use of magnetic biochars for the immobilization of heavy metals in a multi-contaminated soil. Sci Total Environ. 2018; 622–623: 892–899. https://doi.org/10.1016/j.scitotenv.2017.12.056 PMID: 29227940

40. Sekulic MT, Pap S, Stojanovic Z, Boskovic N, Radonic J, Knudsen TS. Efficient removal of priority, hazardous priority and emerging pollutants with Prunus armeniaca functionalized biochar from aqueous wastes: Experimental optimization and modeling. Sci Total Environ. 2018; 613:736–750. https://doi.org/10.1016/j.scitotenv.2017.09.082 PMID: 28938216

41. Bogusz A, Nowak K, Stefaniuk M, Dobrowolski R, Oleszczuk P. Synthesis of biochar from residues after biogas production with respect to cadmium and nickel removal from wastewater. J Environ Manage. 2017; 201:268–276. https://doi.org/10.1016/j.jenvman.2017.06.019 PMID: 28675861

42. Higashikawa FS, Conz RF, Colzato M, Cerri CEP, Alleoni LRF. Effects of feedstock type and slow pyrolysis temperature in the production of biochars on the removal of cadmium and nickel from water. J Clean Prod. 2016; 137:965–972. https://doi.org/10.1016/j.jclepro.2016.07.205

43. Zhang WH, Lo IMC. EDTA-enhanced washing for remediation of Pb- and/or Zn-contaminated soils. J Environ Eng-Asce. 2006; 132(10):1282–8. https://doi.org/10.1061/(asce)0733-9372(2006)132:10 (1282)

44. Lalhruaitluanga H, Jayaram K, Prasad MNV, Kumar KK. Lead(II) adsorption from aqueous solutions by raw and activated charcoals of Melocanna baccifera Roxburgh (bamboo)-A comparative study. J Hazard Mater. 2010; 175(1–3):311–318. https://doi.org/10.1016/j.jhazmat.2009.10.005 PMID: 19883973

45. MOHURD (Ministry of Housing and Urban-Rural Development of China). Disposal of sludge from municipal wastewater treatment plant-Quality of sludge used in forestland. CJ/T 362–2011.

46. Wang X, Li C, Li Z, Yu G, Wang Y. Effect of pyrolysis temperature on characteristics, chemical speciation and risk evaluation of heavy metals in biochar derived from textile dyeing sludge. Ecotox Environ Safe. 2019; 168:45–52. https://doi.org/10.1016/j.ecoenv.2018.10.022.

47. Shen ZT, Zhang YH, Jin F, Alessi DS, Zhang YY, Wang F, et al. Comparison of nickel adsorption on biochars produced from mixed softwood and Miscanthus straw. Environ Sci Pollut R. 2018; 25(15):14626–14635. https://doi.org/10.1007/s11356-018-1674-2 PMID: 29532375

48. Shi YJ, Zhang T, Ren HQ, Kruse A, Cui RF. Polyethylene imine modified hydrochar adsorption for chromium (VI) and nickel (II) removal from aqueous solution. Bioresource Technol. 2018; 247:370–379. https://doi.org/10.1016/j.biortech.2017.09.107 PMID: 28957769

49. Shin WS. Adsorption characteristics of phenol and heavy metals on biochar from Hizikia fusiformis. Environ Earth Sci. 2017; 76(22):782. https://doi.org/10.1007/s12665-017-7125-4

50. Vilvanathan S, Shanthakumar S. Continuous biosorption of nickel from aqueous solution using Chrysanthemum indicum derived biochar in a fixed-bed column. Water Sci Technol. 2017; 76(7):1895–1906. https://doi.org/10.2166/wst.2017.289 PMID: 28991804

51. Lyu HH, Gao B, He F, Zimmerman AR, Ding C, Huang H, et al. Effects of ball milling on the physico-chemical and sorptive properties of biochar: Experimental observations and governing mechanisms. Environ Pollut. 2018; 233:54–63. https://doi.org/10.1016/j.envpol.2017.10.037 PMID: 29053998